An Anti-2D Deceptive Jamming Method for Multi-Baseline Interferometric SAR Based on Co-Localization Jammer

Wenhui Lang, Yaling Tang, Shengqun Mei, Fang Zhou, *Member, IEEE*, and Xuezhi Yang

***Abstract*—Aimed at the problem that range-azimuth joint jamming can effectively generate high fidelity false targets in synthetic aperture radar (SAR) images, an anti-2D deceptive jamming method for multibaseline interferometric SAR is proposed in this article. The method consists of three steps: identification; classification; and suppression. First, the target is detected in the sea clutter background using constant false alarm rate algorithm, and then, the false target is identified base on the difference of the spatial position of the target in different SAR images. Second, through the analysis of the generating principle of deceptive jamming, the false target is classified by multibaseline interferometric SAR according to partial prior knowledge, which is designed based on the differences between the interferometric phase of the true and false target. Finally, the position of the active jammer is co-located underlying the phase equalization characteristics between multiple baselines and the geometric configuration of the SAR, and the adaptive beamforming method is supplied to suppress the jamming signal. The proposed method has a significantly improved ability to suppress jamming relative to interferometric phase cancellation. The effectiveness of the proposed method is verified by simulation.**

***Index Terms*—Anti-2D deceptive jamming, beamforming, jammer positioning, interferometric phase, synthetic aperture radar (SAR).**

I. Introduction

SYNTHETIC aperture radar (SAR) is an active microwave remote sensing system, which can achieve all-day and all-weather high-resolution imaging, and plays a key role in terrain detection, military reconnaissance and other fields [1], [2]. However, SAR system often suffers from complex electromagnetic interference in practical radar imaging. For the purpose of protecting the target from reconnaissance, many jamming methods are designed for SAR system, such as barrage jamming and deceptive jamming [3]. Currently, the antibarrage jamming technology is relatively mature [4]–[6], but deceptive jamming is difficult to identify and suppress since its high fidelity and strong concealment characteristics. Taking effective measures against deceptive jamming is a significant challenge for SAR imaging system.

In general, one-dimensional (1-D) deceptive jamming suppression technology for SAR is divided into two types: single-channel and multichannel SAR suppression technology [7]. About the former, the radar system transmits agile chrip signal to resist deceptive jamming with phase coding modulation, random initial phase or orthogonal frequency division multiplexing [8]–[10]. Nevertheless, due to the different modulation of the transmitting waveform, the difficulty of transmitting and receiving is greatly increased, and the imaging quality of the real target is decreased. In order to solve these problems, Zhao *et al.* [11] suggested that statistical information was used to enhance the difference between real echo and deceptive jamming, and dynamic synthetic aperture and super-resolution schemes were used to realize separation and reconstruction of the real and false targets. About the latter, for example, Li and Zhu [12] and Feng *et al.* [13] detected false targets by obtaining the phase difference of two SAR images with two antennas. But their methods only detect the false target and do not propose method how to suppress it. The multichannel system utilizes the degree of freedom of the space between channels, so that the real signal and the false target have different wave ranges in different channels, and the jamming signal is suppressed by the method of spatial cancellation [14]. However, the real targets in the same direction as jammer are also suppressed in the cancellation process. In [15] and [16], the author recognized the deceptive jamming based on the geometric characteristics of the multistatic SAR and located the position of the jammer through the position relationship between the radar and the false target, so as to realize the antirange deceptive jamming. In brief, 1-D deceptive jamming of a single style can be easily identified and eliminated. With the continuous emergence of the new SAR system, the information processing capability of the SAR system is becoming stronger and stronger, and the 2-D deceptive jamming optimized and combined with the basic interference pattern has gradually become a hot topic [17]–[21]. Therefore, it is necessary and urgent to demonstrate how to effectively resist 2-D deceptive jamming without affecting the real target. At present, the multiple-input and multiple-output synthetic aperture radar (MIMO-SAR) system in [22] used phase compensation to make the real target meet the coherent accumulation, and achieved the suppression of 2-D false targets, but this method requires precise

Manuscript received 19 December 2021; revised 8 March 2022 and 23 April 2022; accepted 15 June 2022. Date of publication 22 June 2022; date of current version 18 July 2022. This work was supported in part by the National Natural Science Foundation of China under Grant 61271381, in part by the Fundamental Research Funds for the Central Universities under Grant JZ2022HGTB0329, and in part by the Aeronautical Science Foundation of China under Grant 2019200P4001. *(Corresponding author: Wenhui Lang.)*

The authors are with the Signal and Information Processing Institute, School of Computer and Information, Hefei University of Technology, Hefei 230009, China (e-mail: langwh@hfut.edu.cn; yltang96@163.com; 2858971834@qq.com; zhoufang@hfut.edu.cn; xzyang@hfut.edu.cn).

Digital Object Identifier 10.1109/JSTARS.2022.3185254

control of the phase, and the imaging of real target might be affected by a slight deviation.

From the above research, it can be found that there are few researches on the anti-2D deceptive jamming of SAR systems. Although 2-D deceptive jamming is difficult to identify with high fidelity characteristics, the degree of freedom of a multichannel SAR system gradually increases with the number of antennas, which also provides more possibilities for us to design antijamming methods. For purpose of extending the degrees of freedom of multichannel SAR, we have introduced the idea of multiview observation on the concept of multibaseline to enhance the ability of multichannel SAR system to identify jamming. Aiming at the problem of how to effectively suppress 2-D deceptive jamming without affecting the imaging of real targets, this article proposes a multibaseline interferometric SAR anti-2D deception jamming method based on co-location and spatial suppression. The method is first to use the constant false alarm rate (CFAR) algorithm to detect the target in the background of sea clutter, and then identifies and classifies the deceptive jamming in the target by estimating the baseline based on partial prior knowledge. Next, a multibaseline interferometric SAR co-location method is designed, which uses the phase equalization characteristics and geometric configuration of the intersection-orbit and along-orbit interferometric SAR to locate the position of the active jammer. Finally, we use the adaptive beamforming method to suppress the incoming signal emitted by the jammer, which enables the suppression of 2-D deceptive jamming.

The rest of this article is organized as follows. In Section II, the deceptive jamming model of multibaseline interferometric SAR is established, and the deceptive jamming of range and azimuth dimension is detected and recognized. Section III classifies deceptive jamming in the azimuth and range dimensions. Section IV presents the method of anti-deceptive jamming, including the location of jammer and the suppression of jamming signal. Section V describes the details of the simulation results and analysis. In Section VI, we briefly summarize this article.

II. Detection and Distinguish of Targets

A. Geometric Model

The system structure of airborne multibaseline interferometric SAR is shown in Fig. 1. SAR platform moves along the $x-$axis with velocity v_a. Antenna A_1 and A_2 represent along-orbit interferometric SAR, while antennas A_1 and A_3 represent intersection-orbit interferometric SAR. The baseline length is denoted by D and S, respectively. Master antenna A_1 and slave antenna A_q ($q = 2, 3, 4$) are the common antennas for transmitting and receiving, where the beam squint angle of antenna A_4 is $\theta_{r,c}$, and the other antennas transmit signals by side-looking mode. When antenna A_1 azimuth slow time $t_a = 0$, the projection point of antenna A_1 on the ground is the coordinate origin. The center of scene is located at $O(0, Y_0)$, point $J(x_j, y_j)$ represents the location of the jammer, and point P' is a false target generated by the jammer modulation. The real target is represented by point P, and the point Q represents the reference points of the real target in the imaging scene.

It is well known that SAR transmits linear frequency modulation signal, and the echo of the target signal received by the

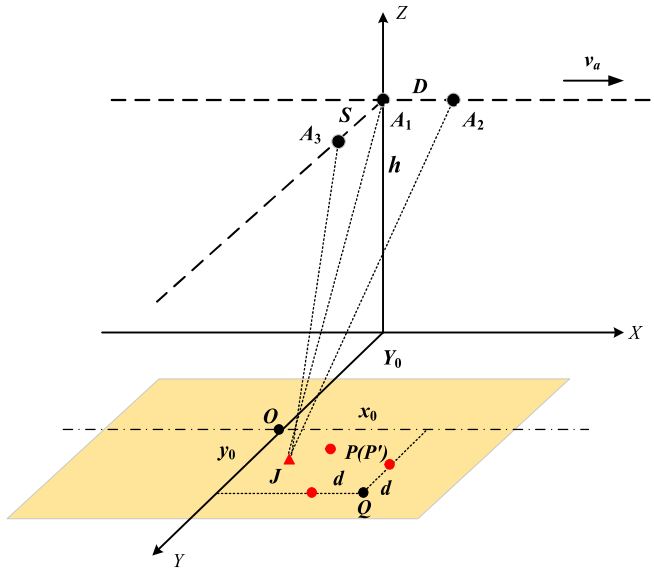

Fig. 1. Deceptive jamming model of multibaseline interferometric SAR.

jammer in the nth channel is expressed as follows [1]:

$$\begin{aligned} s_n(t_r, t_a) &= A_0 w_r\left(t_r - \frac{2R_{jn}(t_a)}{c}\right) w_a(t_a - t_c) \\ &\times \exp\left\{-j2\pi f_0 \frac{2R_{jn}(t_a)}{c}\right\} \\ &\times \exp\left\{j\pi K_r\left(t_r - \frac{2R_{jn}(t_a)}{c}\right)^2\right\} \end{aligned} \tag{1}$$

where t_r and t_a denote fast time and slow time, respectively. $w_r(\cdot)$ is range envelop function, $w_a(\cdot)$ is azimuth envelop function, t_c signifies the azimuth center time, K_r represents the frequency modulation, $R_j(t_a)$ denotes the instantaneous slant distance from radar to jammer, and A_0 represents the scattering intensity of the false target.

B. Identification of Real and False Targets

At present, 2-D deceptive jamming of SAR is mainly generated by azimuth Doppler frequency and range delay modulation [24], [25]. The azimuth Doppler modulation can generate false targets in azimuth dimension, the range delay jamming can generate false targets in range dimension, and the combination of the two can produce 2-D false targets. Therefore, the 2-D deceptive jamming signal intercepted by the jammer is expressed as

$$s_{na}(t_r, t_a) = s_n(t_r, t_a) * \delta(t_r - \tau) \times \exp\left\{j2\pi K_a \frac{\Delta x_j}{v_a} t_a\right\} \tag{2}$$

where Δx_j denotes the azimuth distance from the jammer to the false target; K_a is the azimuth Doppler modulation frequency; τ is the fixed delay. $\delta(\cdot)$ is the Dirac impulse function, and the symbol "$*$" represents convolution.

The 2-D deceptive jamming described above can be decomposed into azimuth-dimension jamming and range-dimension jamming. The generation of SAR azimuth deception jamming is divided into two steps. First, based on the azimuth delay and

Doppler coupling characteristics of the chirp signal, the Doppler modulation of the SAR slow time domain signal is performed. Then, azimuth dimension matching filter is used to generate specific deception jamming in azimuth direction [17]. After omitting the constant term, the antenna A_1 receives the azimuth Doppler modulation jamming signal after focusing, and its the time-domain expression is obtained as

$$s_{1a}(t_r, t_a) = A_0 \sin c\left[\pi B_r\left(t_r - \frac{2r_j}{c}\right)\right] \times \sin c\left[\pi B_a\left(t_a - \frac{x_j}{v_a} + \frac{\Delta x_j}{v_a}\right)\right] \quad (3)$$

where r_j represents the shortest slant distance from radar to jammer, and $r_j = \sqrt{(Y_0 + y_j)^2 + h^2}$. B_r and B_a mean range and azimuth Doppler bandwidth, respectively.

In the SAR imaging scene, range delay jamming commonly used to generate false targets in range dimension [16]. Depending to the expected false target intensity and position information, the jammer performs range delay and amplitude modulation on the intercepted SAR signal. The time domain signal is obtained by focusing the range-delayed jamming echo received by the antenna A_1, and the expression is

$$s_{1r}(t_r, t_a) = A_0 \sin c\left[\pi B_r\left(t_r - \frac{2r_j}{c} - \tau\right)\right] \times \sin c\left[\pi B_a(t_a - t_c)\right]. \quad (4)$$

Obviously, the change of τ and Δx_j can affect the position of the false target. In order to identify false targets in the scene, the radar is allowed to observe the targets from side-looking and squint views respectively. The top view of the multibaseline interferometric SAR is shown in Fig. 2. It is supposed that the point F_1 is the range delay jamming, the point F_2 is the azimuth Doppler modulation jamming, the point F_3 is the 2-D deceptive jamming, and the subscripts $_{r,\ c}$ indicates squint SAR. Since the range delay jamming is generated by fast time forwarding, it is shifted along the range of the jammer and the direction of the radar beam. Therefore, in side-looking and squint SAR, the position of range delay jamming is represented as $F_1(x_j,\ r_j + c\tau\ /\ 2)$ and $F_{1r,c}(x_j + c\tau\sin\theta_{r,c}\ /\ 2,\ r_j + c\tau\cos\theta_{r,c}\ /\ 2)$, respectively. Azimuth dimensional jamming is generated by the jammer through azimuth modulation, which offsets in the azimuthal direction of the jammer and in the vertical direction of the radar beam. Therefore, the false target positions generated by azimuth Doppler jamming are denoted as $F_2(x_j + \Delta x_j,\ r_j)$ and $F_{2r,c}(x_j + \Delta x_j\cos\theta_{r,c},\ r_j - \Delta x_j\sin\theta_{r,c})$ in the side-looking and squint SAR, respectively. Based on the above analysis, The position of the 2-D false target F_3 in different SAR views can be expressed as

$$\begin{cases} x_3 = x_j + \Delta x_j \\ r_3 = r_j + \frac{c\tau}{2} \\ x_{3r,c} = x_j + \Delta x_j\cos\theta_{r,c} + \frac{c\tau}{2}\sin\theta_{r,c} \\ r_{3r,c} = r_j - \Delta x_j\sin\theta_{r,c} + \frac{c\tau}{2}\cos\theta_{r,c} \end{cases} \quad (5)$$

where x_3 and r_3 mean the azimuth coordinates and shortest slant range history of 2-D false target, respectively. x_j and r_j represent the azimuth coordinates of the jammer and the shortest slant distance from radar to jammer, respectively. According to (5), when the observation angle changes, the coordinates of the false target change accordingly, but the coordinates of the real target remain unchanged.

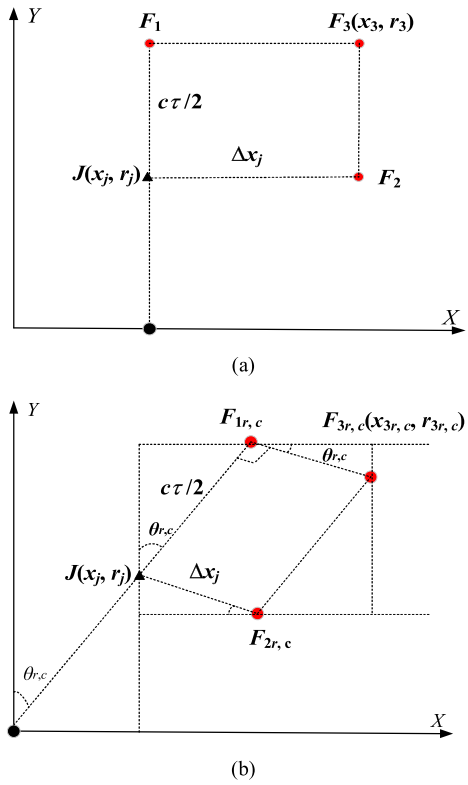

Fig. 2. Top view of side-looking and squint SAR. (a) 2-D geometric model of side-looking SAR. (b) 2-D geometric model of squint SAR.

In order to realize the antideceptive jamming of multibaseline interferometric SAR, it is first necessary to detect the target to be observed in the SAR image. CFAR algorithm is an effective target detection algorithm under the background of sea clutter [23], which can obtain the geometric centers of all the targets of interest in SAR images. Then, based on the same false target has different position offset in SAR images from different perspectives, the false target is identified. we select two images A_i and B_j from SAR images of different viewing angles, where the target geometric center in the A_i image is $\mathbf{A}^{(i)} = \{ai\ 1, ai\ 2, \ldots, ai\ m, \ldots, ai\ M\}$, the target geometric center in the B_i image is $\mathbf{B}^{(j)} = \{bj\ 1, bj\ 2, \ldots, bj\ n, \ldots, bj\ N\}$, $i, j = 1, 2, 3$. Next, the Euclidean Distance between the mth target in A_i and all N targets in B_j in turn, which can be expressed as $\mathbf{d}(i,j)\ m = \{d(i, j)\ m,1, d(i, j)\ m,2, \ldots, d(i, j)\ m,n, \ldots, d(i, j)\ m,N\}$, where $d(i, j)\ m,n$ is calculated as follows:

$$d_{m,n}^{(i,j)} = \sqrt{\left(a_m^i - b_n^j\right)^2}, i \neq j. \quad (6)$$

Finally, we select an appropriate threshold β. When all elements in $\mathbf{d}(i,j)\ m$ are greater than β, it means that the mth target in A_i image is a false target, otherwise it is a real target.

The same operation is repeated on all SAR images from different perspectives to obtain the location distribution of all false targets. According to the corresponding relationship between the delay modulation of the jammer and each false target, the location of the jammer and the suppression of the jamming signal can be realized. The specific implementation details are detailed in Section IV.

III. Classification of Deceptive Jamming

According to the description in Section II, false targets in SAR images can be identified through SAR from different perspectives, but the type of deceptive jamming cannot be judged. Generally, 1-D and 2-D deceptive jamming can be generated by jammer modulation. Through the accurate identification of the false target, the jammer can be located more accurately. In order to further identify false targets, it is also necessary to classify deceptive jamming.

A. Azimuth Deception Jamming Identification

For the azimuth-dimensional deception jamming, the identification principle based on the along-orbit SAR is as follows. As shown in Fig. 1, the instantaneous coordinates of master antenna A_1 and slave antenna A_2 are $(v_a t_a, 0, h)$ and $(v_a t_a + D, 0, h)$ respectively, and the shortest slant distance from radar to scene center O is R_0. We choose a point $Q(x_0, Y_0 + y_0)$ arbitrarily in the scene, assuming that this point is the real target, y_0 represents the range distance from scene center O to point Q, and point $P(P')(x_p, y_p)$ is the unknown target. In order to compare the interferometric phase difference between the point Q and $P(P')$, the instantaneous slant distance from the antenna A_1 to point Q is obtained by Fresnel approximation:

$$R_Q^1(t_a) = \sqrt{(y_0 + Y_0)^2 + (v_a t_a - x_0)^2 + h^2} \approx R_0 + \frac{y_0^2 + 2y_0 Y_0 + (v_a t_a - x_0)^2}{2R_0}. \quad (7)$$

The instantaneous slant distance from antenna A_2 to point Q is

$$R_Q^2(t_a) = \sqrt{(y_0 + Y_0)^2 + (v_a t_a + D - x_0)^2 + h^2} \approx R_0 + \frac{y_0^2 + 2y_0 Y_0 + (v_a t_a + D - x_0)^2}{2R_0}. \quad (8)$$

Thus, the theoretical value of the along-orbit interferometric phase of point Q is as follows:

$$\varphi_{1a} = -\frac{4\pi}{\lambda}\left(R_Q^1(t_a) - R_Q^2(t_a)\right)|_{t_a=0} = \frac{4\pi}{\lambda}\frac{D^2 + 2v_a t_a D - 2Dx_0}{2R_0} = \frac{4\pi}{\lambda}\frac{D^2 - 2Dx_0}{2R_0}. \quad (9)$$

In the actual operation of radar, the attitude error of aircraft is easy to exist, so that the master antenna and the slave antenna are not completely parallel. If along-orbit SAR baseline is too long, the interferometric phase of the real target generates additional phase redundancy, which can be identified as false targets. Before identifying the target, we should first pre-estimate the baseline length of along-orbit interferometric SAR. Assuming that the position of slave antenna A_2 changes linearly with the azimuth at any time, the actual coordinate of antenna A_2 is obtained as $(v_a t_a + (1 + l)D, mD, h + nD)$, where l, m, and n are the rate of change of the deviation in the azimuth, range, and height directions respectively, and$l \ll 1$,$m \ll 1$, $n \ll 1$. Therefore, the true along-orbit interferometric phase at point Q as (10) shown at the bottom of this page, where $a = m^2 + l^2 + 2l + n^2$ and $b = 2nh + 2mY_0 + 2my_0 - 2lx_0$.

Thus, the interferometric phase error caused by the nonparallel radar line-of-sight can be written as

$$\xi_a = \varphi_{1a} - \phi_{1a} = \frac{4\pi}{\lambda}\frac{aD^2 + bD}{2R_0}. \quad (11)$$

Let $|\xi_a| < \eta_a$, where η_a represents the identifiable phase of azimuth direction. Thus, the along-orbit baseline range D can be calculated as

$$[(-b - \sqrt{b^2 + 4a\eta_a\lambda R_0/2\pi})/2a, \; (-b + \sqrt{b^2 + 4a\eta_a\lambda R_0/2\pi})/2a)].$$

Similarly, the theoretical interferometric phase value of point P, whose azimuth distance from point Q is d under the along-orbit interferometric SAR, is calculated as

$$\varphi_{2a} = -\frac{4\pi}{\lambda}\left(R_Q^1(t_a) - R_Q^2(t_a)\right) = -\frac{4\pi}{\lambda}\left(\sqrt{(y_p + Y_0)^2 + (v_a t'_a - x_p)^2 + h^2} - \sqrt{(y_p + Y_0)^2 + (v_a t'_a + D - x_p)^2 + h^2}\right) = \frac{4\pi}{\lambda}\frac{D^2 + 2v_a t'_a D - 2Dx_p}{2R_0}\Big|_{x_p = x_0 + d, t'_a = d/v_a}$$

$$\phi_{1a} = -\frac{4\pi}{\lambda}\left(\sqrt{(Y_0 + y_0)^2 + (v_a t_a - x_0)^2 + h^2} - \sqrt{(Y_0 + mD + y_0)^2 + (v_a t_a + D(1 + l) - x_0)^2 + (h + nD)^2}\right)|_{t_a=0} = -\frac{4\pi}{\lambda}\left(\left(R_Q^1(t_a) - R_Q^2(t_a)\right)|_{t_a=0} - \frac{aD^2 + bD}{2R_0}\right) \quad (10)$$

$$= \frac{4\pi}{\lambda}\frac{D^2 - 2Dx_0}{2R_0}. \tag{12}$$

The true or false of the target can be judged by whether the along-orbit interferometric phase is consistent. For the identification of real targets, it can be obvious known that the azimuth position of point Q is different from point P according to the vector properties of (9) and (12), so the arrival time of the carrier's Doppler center at two points is different. Assuming that radar reaches point Q at Doppler central time $t_a = 0$, the moment at point P is $t_a' = d / v_a$, and substituting it into (12), it can be concluded that (9) is equal to (12), so the along-orbit interferometric phase of real targets is independent of the range direction position of the target. For the identification of false targets in azimuth dimension, point P' is generated by the jammer through azimuth Doppler modulation, and the arrival time of the Doppler center is determined by the position of the jammer. In this case, the azimuth coordinate of point P' is $x_p = x_0 + d$ and the distance between jammer and false target is $\Delta x_j \neq 0$, so $t_a' \neq d / v_a$, namely (9) and (12) are no longer equal. In brief, under along-orbit interferometric SAR, if the interferometric phases of the two targets are the same, then both targets are not affected by the azimuth dimension jamming; otherwise, at least one of the two targets is affected by the azimuth dimension jamming.

B. Range Deception Jamming Identification

In order to identify the range deceptive jamming described above, it is necessary to compare the difference of intersection-orbit interferometric phase between the point Q and $P(P')$. First, the interferometric phase at point Q can be calculated with the instantaneous slant distance of antennas A_1 and A_3 to point Q. As shown in Fig. 1, the instantaneous coordinates of master antenna A_1 and slave antenna A_3 are $(v_a t_a, 0, h)$ and $(v_a t_a, S, h)$, respectively. Assuming that point $P(P')$ is an unknown target, and the range distance between the point Q and the target $P(P')$ is d. The instantaneous slant distance from antenna A_1 to point Q is

$$\begin{aligned} R_Q^1(t_a) &= \sqrt{(y_0+Y_0)^2 + (v_a t_a - x_0)^2 + h^2} \\ &\approx R_0 + \frac{y_0^2 + 2y_0 Y_0 + (v_a t_a - x_0)^2}{2R_0}. \end{aligned} \tag{13}$$

The instantaneous slant distance from antenna A_3 to point Q is

$$\begin{aligned} R_Q^3(t_a) &= \sqrt{(y_0 + Y_0 - S)^2 + (v_a t_a - x_0)^2 + h^2} \\ &\approx R_0 + \frac{y_0^2 + 2y_0 Y_0 + S^2 - 2y_0 S - 2Y_0 S + (v_a t_a - x_0)^2}{2R_0}. \end{aligned} \tag{14}$$

Thus, the theoretical value of the intersection-orbit interferometric phase of point Q is

$$\begin{aligned} \varphi_{1r} &= -\frac{4\pi}{\lambda}\left(R_Q^1(t_a) - R_Q^3(t_a)\right) \\ &= -\frac{4\pi}{\lambda}\left(\sqrt{(y_0+Y_0)^2 + (v_a t_a - x_0)^2 + h^2}\right. \\ &\quad \left. - \sqrt{(y_0 + Y_0 - S)^2 + (v_a t_a - x_0)^2 + h^2}\right) \\ &= \frac{4\pi}{\lambda}\left(\frac{S^2 - 2y_0 S - 2Y_0 S}{2R_0}\right). \end{aligned} \tag{15}$$

Then, the theoretical interferometric phase value of point P, whose range distance from the point Q is d under intersection-orbit interferometric SAR, is calculated as

$$\begin{aligned} \varphi_{2r} &= -\frac{4\pi}{\lambda}\left(R_Q^1(t_a) - R_Q^3(t_a)\right) \\ &= -\frac{4\pi}{\lambda}\left(\sqrt{(y_p+Y_0)^2 + (v_a t_a - x_p)^2 + h^2}\right. \\ &\quad \left. -\sqrt{(y_p + Y_0 - S)^2 + (v_a t_a - x_p)^2 + h^2}\right) \\ &= \frac{4\pi}{\lambda}\left(\frac{S^2 - 2y_p S - 2Y_0 S}{2R_0}\right)\Big|_{y_p = y_0 + d} \\ &= \frac{4\pi}{\lambda}\left(\frac{S^2 - 2dS - 2Y_0 S - 2y_0 S}{2R_0}\right). \end{aligned} \tag{16}$$

If the point $Q(x_p + d, y_p)$ is located at the azimuth interval d from the unknown target $P(P')$, the theoretical value of the intersection-orbit interferometric phase at point Q is

$$\begin{aligned} \varphi_{2a} &= -\frac{4\pi}{\lambda}\left(R_Q^1(t_a) - R_Q^3(t_a)\right) \\ &= -\frac{4\pi}{\lambda}\left(\sqrt{(y_p + Y_0)^2 + (v_a t_a - x_p - d)^2 + h^2}\right. \\ &\quad \left. - \sqrt{(y_0 + Y_0 - S)^2 + (v_a t_a - x_p - d)^2 + h^2}\right) \\ &= \frac{4\pi}{\lambda}\left(\frac{S^2 - 2y_p S - 2Y_0 S}{2R_0}\right). \end{aligned} \tag{17}$$

Obviously, under intersection-orbit interferometric SAR, it can be seen that $\varphi_{1r} \neq \varphi_{2r}$ from (15) and (16), which shows that interferometric phase of the true target along the range direction is not equal. Base on (16) and (17), it can be seen that the interferometric phase of the true target along the azimuth direction is equal. Therefore, the true or false of the targets can be judged according to whether the intersection-orbit interferometric phase are consistent.

For the identification of real targets, it can be obvious known that the range position of point Q is different from point P according to the vector properties of (15) and (16), so the instantaneous slant distances from the radar to the two points are also different, and it can be concluded that (15) and (16) are not equal. For the discrimination of false target produced by range delay modulation, since the range delay jamming is generated by the jammer through the fast time delay τ forwarding, it does not affect the slant distance history of the false target. Therefore, the intersection-orbit interferometric phases of the false targets generated by the range delay are all equal, and this method is suitable for situations where there are n false targets in the scene

($n \geq 2$, n represents the number of false targets). In short, if the interferometric phases of multiple targets along the range direction are the same, it can be judged that the target is range delay jamming; otherwise, the target is a real target.

Similarly, the attitude error also exists in the intersection-orbit SAR, which can cause the radar's line of sight to be nonparallel. Taking the master A_1 antenna as a reference, if the baseline of intersection-orbit SAR is too long, the actual movement of the slave antenna A_3 deviates from the ideal trajectory, so that the interferometric phase of the targes can be aliased. In order to identify deceptive jamming effectively, the baseline length should be estimated first. It is assumed that the true coordinate of the antenna A_3 is $(v_a t_a + mS, (1+l)S, h+nS)$ at any time, and the true intersection-orbit interferometric phase of point Q as (18) shown at the bottom of this page, where $c = 2nh - 2lY_0 - 2mx_0 - 2ly_0$. Therefore, it is necessary to minimize the interferometric phase error caused by non-parallel radar line of sight as follows:

$$\xi_r = \varphi_{1r} - \phi_{1r} = \frac{4\pi}{\lambda}\left(\frac{aS^2 + cS}{2R_0}\right). \tag{19}$$

Let $|\xi_r| < \eta_r$, where η_r represents the phase identifiable in the range domain, and the baseline range S for intersection-orbit SAR can be calculated as $[(-c - \sqrt{c^2 + 4a\eta_r\lambda R_0/2\pi})/2a, (-c + \sqrt{c^2 + 4a\eta_r\lambda R_0/2\pi})/2a]$.

Obviously, if the baseline is too short, the interferometric phase of true targets in different range directions are consistent, and the range delay jamming cannot be recognized. If the baseline is too long, the limit average number of sights in the range of the radar observation area can be inconsistent [27]. For purpose of further optimizing the length of the baseline and improve the detection accuracy of false target, it can be achieved by maximizing the phase difference φ_{12r} of the intersection-orbit interferometric of the true target as shown in (20). This formula satisfies the two constraints of and ① and ②, where ① means that the limit average number of sights in the range of antenna A_3 is equal to that of antenna A_1; ② indicates that the intersection-orbit interferometric phase difference of the true target's is greater than the recognizable phase

$$\begin{cases} \max \varphi_{12r} = \varphi_{1r} - \varphi_{2r} \\ \text{s.t. } ① \left\lceil \frac{X_a/2 + (R_0 - S_{\max})\theta_{bw} PRF}{v_a} \right\rceil = \left\lceil \frac{X_a/2 + R_0\theta_{bw} PRF}{v_a} \right\rceil \\ \quad ② \ \varphi_{12r} > \eta_r \end{cases} \tag{20}$$

where X_a denotes the azimuth width of the SAR scene, PRF stands for pulse repetition frequency, θ_{bw} is beam width, $S_{\max}$ represents the maximum baseline length of intersection-orbit SAR, and $\lceil\ \rceil$ represents rounding up.

IV. Jammer Location and Jamming Signal Suppression

A. Azimuth Position of Jammer

In the case of along-orbit interferometric SAR, master antenna A_1 transmits signals, and slave antenna A_1 and A_2 receive signals. The equivalent phase centers of different channels are different, and the phase equalization can keep the phase consistency of true echoes received by different channels. Through the along-orbit interferometric cancellation, the real target and the false target generated by range delay jamming can be eliminated in the SAR image, while the false target generated by azimuth jamming can be retained. The range dimension jamming takes the range delay as an example [16]. After omitting the constant term, the antenna A_2 receives the jamming signal after focusing as follows:

$$\begin{aligned} s_{2r}(t_r, t_a) = A_0 \operatorname{sinc}\left[\pi B_r\left(t_r - \frac{2r_j}{c} - \tau\right)\right] \operatorname{sinc}\left[\pi B_a (t_a - t_c)\right] \\ \times \exp\left(-j\frac{2\pi}{\lambda}\left(\frac{2x_F D + D^2}{r_F} - \frac{Dv_a t_a}{r_F}\right)\right) \end{aligned} \tag{21}$$

where (x_F, y_F) denotes the coordinates of the false target and r_F represents the shortest slant range from the radar to the false target.

Due to the position deviation of each receiving channel along the track direction, before interferometric cancellation, slave antenna A_2 needs to compensate for the phase deviation caused by the different channel positions and the Doppler center frequency deviation caused by the baseline interval, so the compensated phase φ_a can be expressed as

$$\varphi_a = \exp\left\{-j\pi\frac{2Dv_a t_a}{\lambda r_F}\right\} \times \exp\left\{j2\pi\frac{D^2 + 2Dx_F}{\lambda r_F}\right\}. \tag{22}$$

We can identify the range jamming through the intersection-orbit interferometric SAR described in Section III-B, and the false target interferometric phase generated by the delay modulation along the same range direction of the jammer is consistent. Therefore, if there are n ($n \geq 2$) targets along the same distance in the scene with the same interferometric phase, the target can be judged as deceptive jamming. Then the compensation phase φ_a of the signal received by antenna A_2 is cancelled with the signal received by antenna A_1 in Section II, so that the false targets in the same range dimension with the jammer can meet the coherent accumulation, and the false targets in the same azimuth dimension with the jammer can meet the incoherent accumulation. In this way, the deceptive jamming of the same range dimension as the jammer is suppressed, and

$$\begin{aligned} \phi_{1r} = & -\frac{4\pi}{\lambda}\left(\sqrt{(Y_0 + y_0)^2 + (v_a t_a - x_0)^2 + h^2}\right. \\ & \left. -\sqrt{(Y_0 - S(1+l) + y_0)^2 + (v_a t_a + mS - x_0)^2 + (h + nS)^2}\right)|_{t_a = 0} \\ = & -\frac{4\pi}{\lambda}\left(\left(R_Q^1(t_a) - R_Q^3(t_a)\right)|_{t_a=0} - \frac{aS^2 + cS}{2R_0}\right) \end{aligned} \tag{18}$$

the deceptive jamming of the same azimuth dimension as the jammer is retained, so the azimuth coordinates of the jammer can be obtained as $x_j = x_F$.

B. Range Position of Jammer

In the case of intersection-orbit interferometric SAR, master antenna A_1 transmits signals, slave antennas A_1 and A_3 receive signals. The range location of jammer is realized by intersection-orbit interferometric SAR, which can eliminate the false targets generated by azimuth Doppler modulation jamming and keep the false targets generated by range delay jamming. Here, we use azimuth Doppler modulation as azimuth dimensional jamming [17]. Antenna A_3 receives jamming signal after focusing can be expressed as:

$$\begin{aligned} s_{3a}(t_r, t_a) = {} & A_0 \sin c\left[\pi B_r\left(t_r - \frac{2r_j}{c}\right)\right] \\ & \times \sin c\left[\pi B_a\left(t_a - \frac{x_j}{v_a} + \frac{\Delta x_j}{v_a}\right)\right] \\ & \times \exp\left(-j\frac{2\pi}{\lambda}\frac{S^2 - 2y_F S - 2SY_0}{r_F}\right). \end{aligned} \tag{23}$$

Due to the position deviation of each receiving channel across the track direction, it is necessary to compensate the phase before the interferometric phase cancellation. The phase of the antenna A_3 to be compensated is related to the position of the azimuth-dimensional deceptive jamming, and the corresponding compensation function is

$$\varphi_r = \exp\left\{-j2\pi\left(\frac{2y_F S + 2SY_0 - S^2}{\lambda r_F}\right)\right\}. \tag{24}$$

We can identify azimuth Doppler modulation jamming and real targets by using along-orbit interferometric SAR described in Section III-A, and the false target interferometric phase generated by the azimuth Doppler modulation along the same azimuth of the jammer is inconsistent. Therefore, if there are n ($n \geq 2$) targets along the same azimuth in the scene with inconsistent interferometric phases, the target can be judged to be deceptive jamming. Then the compensation phase φ_r of the signal received by antenna A_3 is cancelled with antenna A_1 in Section II, so that the jamming signal in the same azimuth dimension with the jammer can meet the coherent accumulation, and the other signals can meet the noncoherent accumulation. In this way, the deceptive jamming signals in the same azimuth dimension as jammer and the real target are suppressed, and the deceptive jamming signals in the same range dimension as the jammer are retained. Thus, we can get the range position of the jammer is $y_j = y_F$.

C. Two-Dimensional Position of Jammer

If there is no 1-D deceptive jamming in the scene, the position of the jammer cannot be accurately known only by the interferometric phase of the target and interferometric cancellation. According to the analysis in Section III, along-orbit interferometric SAR can identify whether the false target is interfered by azimuth-dimension modulation, and intersection-orbit interferometric SAR can identify whether the false target is interfered by range-dimension modulation. Therefore, we can judge the combination type of 2-D deceptive jamming through combination of along-orbit and intersection-orbit interferometric SAR. In order to further determine the location of the jammer, it is also necessary to have the SAR observe the target from different viewpoints after the type of jamming of the false target has been determined. The geometric relationship for 2-D deceptive jamming from different SAR perspectives can be expressed as

$$\begin{cases} x_F^i = x_j^i + \Delta x_j \cos\theta_q + \frac{c\tau}{2}\sin\theta_q \\ r_F^i = r_j^i - \Delta x_j \sin\theta_q + \frac{c\tau}{2}\cos\theta_q \end{cases} \tag{25}$$

where (x_F^i, r_F^i) denote the coordinates of the false target generated by the jammer in the ith SAR image, and $i = 1, 2, 3$. q represents different oblique angles of radar, and $q = 0^\circ, 10^\circ, 22^\circ$. By solving the above equations, the position of the jammer can be obtained as (x_j, y_j).

D. Deceptive Jamming Suppression

Based on the geometric configuration of the multibaseline interferometric SAR, we obtained the position of the jammer and suppressed the deceptive jamming by interferometric cancellation. However, the false targets near the jammer have strong scattering characteristics, and some of the drag shadows of the jamming remain after interferometric cancellation, while the real target signals in the same azimuth dimension as the jammer can be suppressed. Therefore, the antijamming effect of the interferometric cancellation method is not satisfactory. For the purpose of increasing the flexibility of the SAR, multibaseline interferometric SAR is equipped with array antennas. The digital beamforming adjusts the weighting coefficient of each array according to certain criteria to ensure the beam direction, so that the radar can set zero trapped in the specified direction of the antenna pattern. In this process, the jamming signal emitted by the jammer is suppressed.

Linear constrained minimum variance criterion beamforming [26] is selected to suppress the jamming signals in this article. Assuming that there are K complex signals $\mathbf{s}(\cdot)$ in the receiving space, which are shot into the array at different angles and the number of receiving antennas is N, then the array expression for the received signal is

$$\mathbf{y}(t_r, t_a) = \sum_{i=1}^{K} \mathbf{s}(t_r, t_a, i)\mathbf{a}(\theta_i) + \mathbf{n}(t_r, t_a, i) \tag{26}$$

where $\mathbf{a}(\theta) = [1, \exp^{j2\pi d\sin\theta/\lambda}, \cdots, \exp^{j2\pi(K-1)d\sin\theta/\lambda}]^T \in \mathbb{C}^{K\times 1}$ represents array steering vector, reflecting the phase difference of the complex signal arriving at different antennas, $\mathbf{n}(\cdot)$ denotes signal noise.

Assuming that we are only interested in the incoming wave $\mathbf{s}_d(t_r, t_a)$ in the θ_d direction and wish to suppress jamming signals in the other θ_j directions, then the receiving signal from radar

array antenna can be written as

$$\mathbf{y}(t_r,t_a)=\mathbf{s}_d(t_r,t_a)\,\mathbf{a}(\theta_d)+\sum_{i=1}^{K-1}\mathbf{s}_j(t_r,t_a,i-1)\mathbf{a}(\theta_j)+\mathbf{n}(t_r,t_a,i). \tag{27}$$

The existing adaptive weight $\mathbf{w}\in\mathbb{C}^{N\times 1}$ acts on radar array signal, and after adaptive filtering, the average power of output signal is

$$P=E\left(\left|\mathbf{w}^H\mathbf{y}\right|^2\right)=\mathbf{w}^H\mathbf{R}\mathbf{w} \tag{28}$$

where $\mathbf{R}\in\mathbb{C}^{N\times N}$ represents the spatial correlation matrix of the input signal of the radar array, ^{H} denotes the conjugate transposition, and the optimal estimation is obtained by minimizing the output signal power as follows:

$$\begin{cases}\min \mathbf{w}^H\mathbf{R}\mathbf{w}\\ \text{s.t. } \mathbf{A}^{\mathbf{H}}(\theta)\,\mathbf{w}=\mathbf{f}\end{cases} \tag{29}$$

where $\mathbf{A}(\theta)=[\mathbf{a}(\theta_d),\mathbf{a}(\theta_j),\cdots,\mathbf{a}(\theta_{N-1})]\in\mathbb{C}^{K\times N}$. To ensure that the desired signal is not distorted, jamming signal is suppressed by setting zero point. Let$\mathbf{f}=[1,0,\cdots,0]^T\in\mathbb{R}^{K\times 1}$, the optimal weight $\mathbf{w_{opt}}\in\mathbb{C}^{N\times 1}$of (29) is solved by Lagrange's equation as follows:

$$\mathbf{w_{opt}}=\mathbf{R}^{-1}\mathbf{A}(\theta)\left(\mathbf{A}^H(\theta)\,\mathbf{R}^{-1}\mathbf{A}(\theta)\right)^{-1}\mathbf{f}^H. \tag{30}$$

After the above steps, the position of the jammer can be located according to the relationship between the jammer, the jamming characteristics of the false target and the different radar viewing angles, and the jamming signal can be suppressed at the same time. The specific flow chart of the proposed method is shown in Fig. 3.

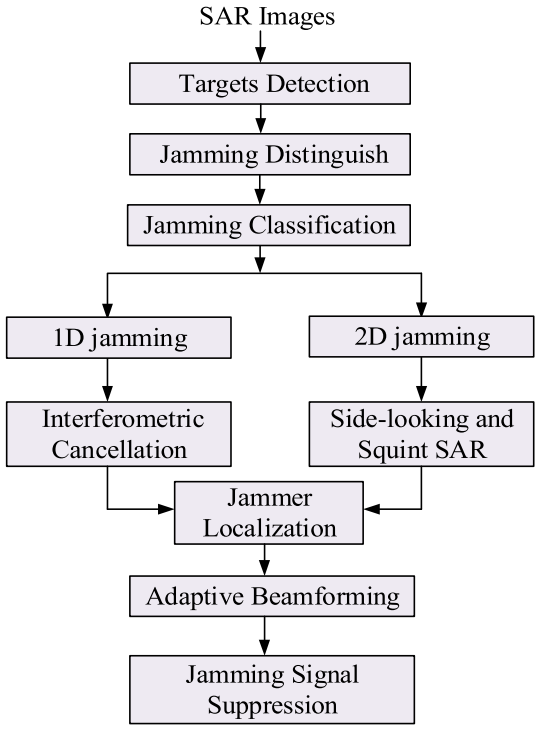

Fig. 3. Flowchart of the proposed method.

V. Simulation and Analysis

In the simulation experiment, the multibaseline interferometric SAR system observes the target from different perspectives, and identifies the deceptive jamming types by using the interferometric phase characteristics of along-orbit and intersection-orbit SAR. In this article, ten ships near the coastline were selected as the simulation scene to prove the effectiveness of the proposed method. The original scene is shown in Fig. 4(a), *x*-axis represents azimuth direction and *y*-axis represents range direction. The simulation parameters are given in Table I.

TABLE I
SAR Parameter Settings

Parameters	Values
Carrier frequency	5.3 GHz
Closest range	12 km
Chirp rate	10^{14}
Signal bandwidth	150 MHz
Beam width	0.03 rad
Pulse width	1.5 us

The jammer puts the template of the ship into the digital radio frequency memory (DRFM) memory in advance, and generates false targets through azimuth-range joint modulation as shown in Fig. 4(b). The false targets in the scene include 1-D and 2-D deceptive jamming. The simulation experiment mainly consists of two parts. One is the identification and suppression of deceptive jamming. First, the SAR is allowed to observe the target from three different perspectives. Second, the type of deceptive jamming in the scene is identified by multibaseline interferometric SAR, then the location of the jammer is located according to the location of the false target in different SAR images, and suppress the jamming by using interferometric cancellation and adaptive beamforming methods. Finally, the SAR image without jamming is obtained. The other is quantitative analysis. This article chooses the signal-to-interference ratio to measure the jamming suppression effect, and signal-to-interference ratio of interferometric cancellation and adaptive beamforming is listed. Ultimately, the antijamming performance of the proposed method is analyzed.

A. Identification and Classification of Deceptive Jamming

In the environment of sea clutter, OR-CFAR algorithm is selected to detect targets in SAR images and obtain the geometric center of the target of interest. In this simulation, ships were considered objects of interest. First of all, it is clear from the geometrical characteristics of the side-looking and squint SAR that when the observation angle changes, the position of the false target changes, but the coordinates of the real target remain unchanged. Therefore, we let SAR observe the target from

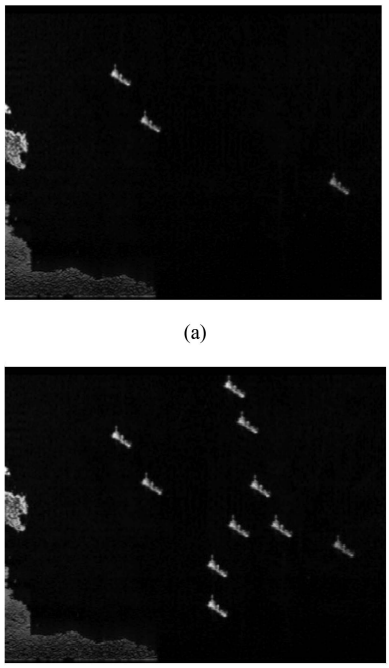

(a)

(b)

Fig. 4. Original scene and false targets. (a) Original scene. (b) False targets.

three different angles: 0°; 10°; and 22°, and the experimental simulation are shown in Fig. 5(a)–(c). The true target is marked with a green box, and the false target is marked with a red box.

According to the red box mark in Fig. 5, it shows that there are seven false targets in the SAR image, but the type of deceptive jamming cannot be distinguished. To further identify false targets, we use a priori knowledge to select the baseline lengths of $S = 14$ m and $D = 4$ m for intersecting-orbit and along-orbit SAR respectively, and then judge the deceptive jamming type base on the interferometric phase of the target. In general, deceptive jamming is divided into two categories. One is 1-D deceptive jamming, which mainly includes range delay and azimuth Doppler modulation jamming. The other is 2-D deceptive jamming, which is mainly a combination of 1-D jamming. In real scene imaging, 1-D deceptive jamming is generally along the same azimuth or range from the jammer, or along the direction of the radar beam and the vertical direction of the beam. and the 2-D deceptive jamming is scattered around the jammer. From the along-orbit interferometric SAR in Fig. 6(a), the interferometric phase of real targets 1, 2, and 3 is consistent with the interferometric phase of false targets 4 and 5 generated by the range delay jamming, and they are all displayed in light green. In the intersection-orbit interferometric SAR of Fig. 6(b), it can be seen that interferometric phase 4, 5, 8, 9, and 10 with range delay are consistent with the 1-D azimuth jamming 6, 7, so they show the same color. The interferometric phases of the real targets 1, 2, and 3 are not consistent, so the colors are not consistent. Therefore, we can identify the deceptive jamming types of false targets based on along-orbit and intersection-orbit SAR, and the target recognition result is shown in Fig. 6(c). 1-D deceptive jamming is marked with a yellow box, and 2-D deceptive jamming is marked with a red box. The classification results of the targets are given in Tables II and III. It can be seen from the table that a single intersection-orbit SAR or along-orbit SAR cannot identify all types of deceptive jamming, and the black "$\surd$" indicates a possible misjudgment result. Therefore, it is necessary to combine the two interferometric SAR methods, and the intersection of the obtained results is the correct identification result, as shown by the red "$\surd$" in Tables II and III.

B. Suppression of Deceptive Jamming

After the above analysis, if there is 1-D deceptive jamming in the scene, the position of the jammer can be quickly located using the interferometric phase characteristics of the false target. By analyzing Fig. 6(a) and (b), we can know which targets in the SAR image are 1-D deceptive jamming. Generally, the range delay jamming and the jammer are in the same azimuth dimension, such as the common azimuth coordinates with targets 4 and 5. The azimuth Doppler modulation jamming and the jammer are in the same distance dimension, for example, it has the same range coordinates with targets 6 and 7. Therefore, by observing the interferometric phase diagram of the target, it can be known that the position of the jammer is (19.5, -10.5) in Fig. 6(c). If there is only 2-D deceptive jamming exists in the scene, the position of the false target under different SAR perspectives can be known from Fig. 5(a)–(c), and then by solving (25), the position of the jammer can be calculated as (19.65, -9.86).

In order to verify the jamming suppression performance of the adaptive beamforming method for active jammer positioning, we compared it with interferometric cancellation antijamming. As can be seen in Fig. 7(a), the along-orbit interferometric cancellation is able to suppress the range delay jamming 4 and 5, but the real targets 1, 2, and 3 is corrupted. In Fig. 7(b), the intersection-orbit interferometric cancellation is able to suppress the azimuth Doppler modulation jamming 6 and 7, but it is not effective for other types of deceptive jamming. In Fig. 7(c), the combined interferometric cancellation of along-orbit and intersection-orbit SAR has a good effect on 1-D deceptive jamming suppression, but the suppression effect on 2-D deceptive jamming 8, 9, and 10 is poor. In general, interferometric cancellation is better at suppressing the amplitude of 1-D deceptive jamming, but it destroys the real target and cannot well weaken the amplitude of 2-D deceptive jamming. In this article, the adaptive beam method of jammer positioning can effectively suppress the jamming signal. The SAR images in Fig. 7(d) show that the deceptive jamming is basically completely suppressed, and the real targets 1, 2, and 3 are well preserved.

C. Antideceptive Jamming Performance Evaluation

To demonstrate the effectiveness of the proposed method, the ratio of required signal power to interference power is used as an indicator, which is called signal interference ratio (SIR), as follows:

$$SIR = 10\log_{10}\frac{\sum_{p,q}|D(x_p,y_q)|^2}{\sum_{p,q}|Y(x_p,y_q)|^2} \tag{31}$$

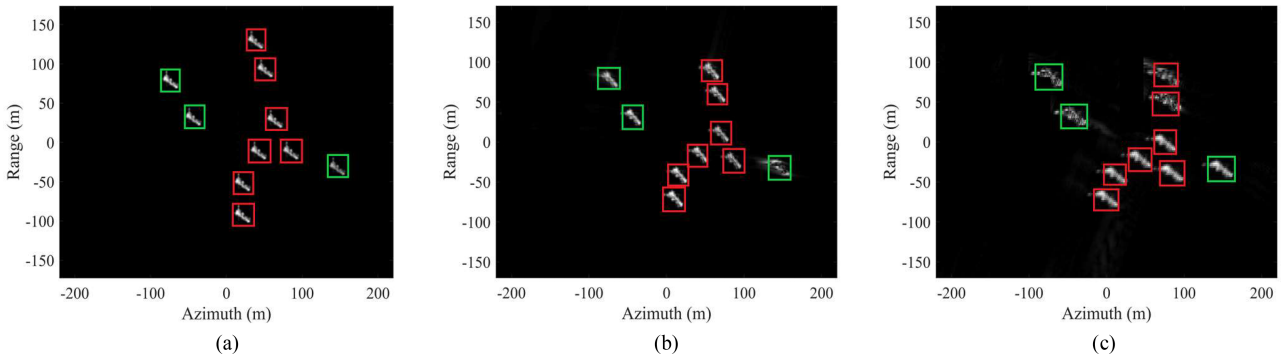

Fig. 5. Different perspectives of SAR. (a) 0°. (b) 10°. (c) 22°.

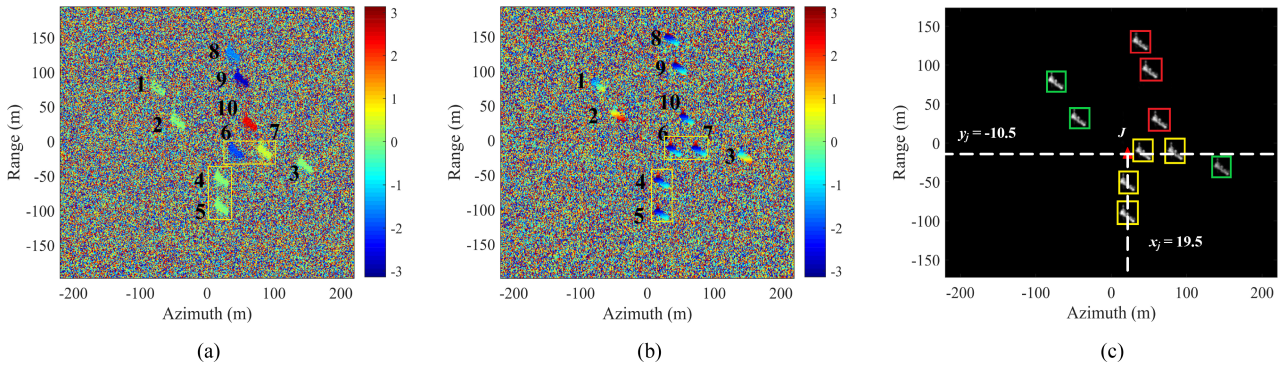

Fig. 6. Classification of false targets. (a) Along-orbit interferometric phase. (b) Intersection-orbit interferometric phase. (c) Recognition result.

TABLE II
RECOGNITION RESULTS OF ALONG-ORBIT INTERFEROMETRIC SAR

Type	Target 1	Target 2	Target 3	Target 4	Target 5	Target 6	Target 7	Target 8	Target 9	Target 10
Range delay				√	√					
Azimuth Doppler						√	√			
2-D-jamming								√	√	√
True target	√	√	√	√	√					

TABLE III
RECOGNITION RESULTS OF INTERSECTION-ORBIT INTERFEROMETRIC SAR

Type	Target 1	Target 2	Target 3	Target 4	Target 5	Target 6	Target 7	Target 8	Target 9	Target 10
Range delay				√	√					
Azimuth Doppler						√	√			
2-D-jamming								√	√	√
True target	√	√	√			√	√			

where $Y(\cdot)$ represents the scattering coefficient of images after processing. $D(\cdot)$ represents the scattering coefficient of an image containing jamming. p and q denote the number of pixels in the azimuth direction and the range direction, respectively. The larger the SIR, the better the antijamming performance. The anti-jamming performance evaluation of interferometric cancellation and adaptive beamforming methods is given in Table IV.

It can be seen from Table IV that compared with interferometric cancellation, the adaptive beamforming method of jammer positioning not only improves the suppression effect of 1-D deceptive jamming, but also significantly enhances the ability to suppress 2-D deceptive jamming.

To further judge the performance of the proposed method in suppressing 2-D deceptive jamming, it is assumed that there

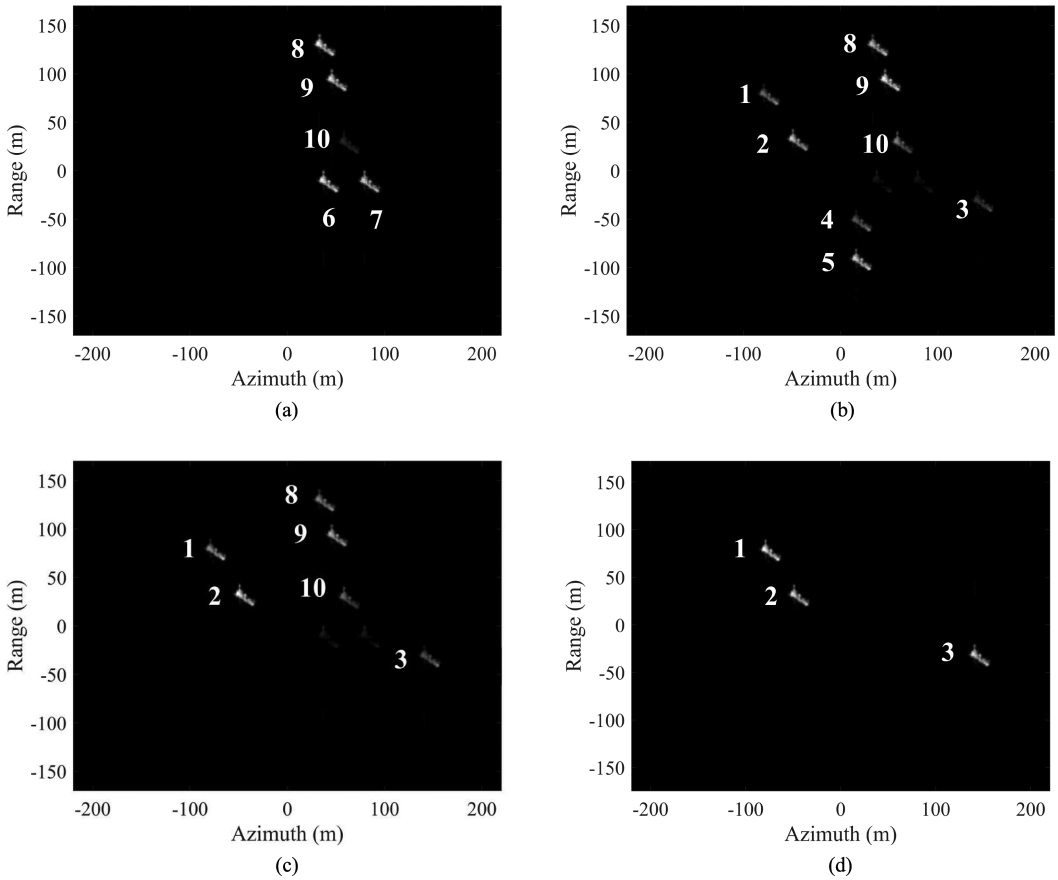

Fig. 7. Suppression of deceptive jamming. (a) Along-orbit SAR interferometric cancellation. (b) Intersection-orbit SAR interferometric cancellation. (c) Along-orbit and intersection-orbit SAR joint interferometric cancellation. (d) The proposed method.

TABLE IV
ANALYSIS OF ANTIDECEPTIVE JAMMING PERFORMANCE

Type of jamming	SIR^0 (Original)	SIR^1 (Interferometric cancellation)	SIR^2 (Proposed method)
Range delay jamming	-10.2023	9.7017	10.3013
Azimuth Doppler jamming	-10.9830	7.2565	10.8840
2-D-jamming[1]	-8.3193	1.9155	8.4192
2-D-jamming[2]	-8.1556	2.3500	9.1894

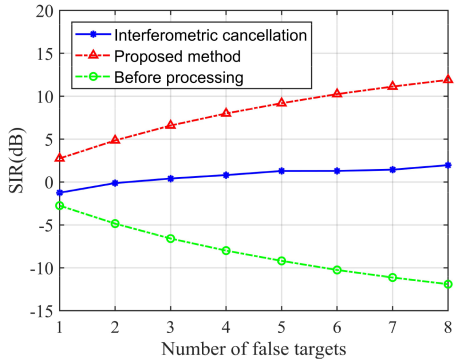

Fig. 8. Performance analysis of deceptive jamming suppression.

are only two real targets in the scene, and the number of 2-D false targets is constantly changing. Then, the antijamming SIR values of the jammer positioning adaptive beamforming and interferometric cancellation are evaluated respectively, and the experimental simulation is shown in Fig. 8. After the jamming signal suppression, the SIR value has been improved. However, compared with interferometric cancellation, when the number of false targets increases, the SIR value of the adaptive beamforming method for jammer positioning to suppress jamming is significantly higher. According to the above analysis, the proposed method has better anti-jamming performance, which not only effectively eliminates 2-D false targets, but also does not affect the imaging of real targets.

VI. CONCLUSION

In order to effectively suppress high-fidelity 2-D deceptive jamming in SAR images, a multibaseline interferometric SAR anti-2D deceptive jamming method is proposed in this article. The method first uses CFAR algorithm to detect the position information of the target to be observed under the background of sea clutter, and then designs an optimal baseline interferometric

SAR to identify 2-D deceptive jamming based on partial a priori knowledge. Finally, the geometric characteristics of the multibaseline interferometric SAR are used to co-locate the position of the active jammer.

For the positioning of the jammer, we considered two jamming scenarios. One is that the false target contains 1-D deceptive jamming, and the range and azimuth positions of the jammer are located separately by using the along-orbit and intersection-orbit SAR interferometric cancellation respectively, while still suppressing most of the interference. The other is that there is only 2-D deceptive jamming in the scene, and the position of the jammer is located from different perspectives through side-looking SAR and squint SAR. After obtaining the position information of the jammer, the SAR is equipped with an array antenna, and then, the adaptive beamforming method is used to suppress the jamming signal emitted by the jammer. As the future work, we will further study the multibaseline interferometric SAR antiscattered wave deceptive jamming.

REFERENCES

[1] I. G. Cumming and F. H. Wong, *Digital Signal Processing of Synthetic Aperture Radar Data: Algorithms and Implementation*. Boston, MA, USA: Artech House, 2005.

[2] H. Sun, M. Shimada, and F. Xu, "Recent advances in synthetic aperture radar remote sensing—Systems, data processing, and applications," *IEEE Geosci. Remote Sens. Lett.*, vol. 14, no. 11, pp. 2013–2016, Nov. 2017.

[3] Q. Sun, T. Shu, M. Tang, K. Yu, and W. Yu, "Effective moving target deception jamming against multichannel SAR-GMTI based on multiple jammers," *IEEE Geosci. Remote Sens. Lett.*, vol. 17, no. 3, pp. 441–445, Mar. 2020.

[4] F. Zhou, R. Wu, M. Xing, and Z. Bao, "Eigensubspace-based filtering with application in narrow-band interference suppression for SAR," *IEEE Geosci. Remote Sens. Lett.*, vol. 4, no. 1, pp. 75–79, Jan. 2007.

[5] J. Feng, H. Zheng, Y. Deng, and D. Gao, "Application of subband spectral cancellation for SAR narrow-band interference suppression," *IEEE Geosci. Remote Sens. Lett.*, vol. 9, no. 2, pp. 190–193, Mar. 2012.

[6] F. J. Meyer, J. B. Nicoll, and A. P. Doulgeris, "Correction and characterization of radio frequency interference signatures in L-band synthetic aperture radar data," *IEEE Trans. Geosci. Remote Sens.*, vol. 51, no. 10, pp. 4961–4972, Oct. 2013.

[7] X. Lu, Y. Zhao, J. Yang, W. Su, H. Gu, and T. S. Yeo, "An efficient method for single-channel SAR target reconstruction under severe deceptive jamming," *IEEE Geosci. Remote Sens. Lett.*, vol. 17, no. 2, pp. 237–241, Feb. 2020.

[8] X. Qiu, T. Zhang, S. Li, T. Yuan, and F. Wang, "SAR anti-jamming technique using orthogonal LFM-PC hybrid modulated signal," in *Proc. China Int. SAR Symp.*, 2018, pp. 1–6.

[9] Q. Feng, H. Xu, Z. Wu, and B. Sun, "Deceptive jamming suppression for SAR based on time-varying initial phase," in *Proc. IEEE Int. Geosci. Remote Sens. Symp.*, 2016, pp. 4996–4999.

[10] Y. Li, X. Jia, Y. Chen, and C. Yin, "Frequency agility MIMO-SAR imaging and anti-deception jamming performance," in *Proc. URSI Gen. Assem. Sci. Symp.*, 2014, pp. 1–4.

[11] B. Zhao, L. Huang, and J. Zhang, "Single channel SAR deception jamming suppression via dynamic aperture processing," *IEEE Sensors J.*, vol. 17, no. 13, pp. 4225–4230, Jul. 2017.

[12] C. Li and D. Zhu, "The detection of deception jamming against SAR based on dual-aperture antenna cross-track interferometry," in *Proc. CIE Int. Conf. Radar.*, 2016, pp. 1–4.

[13] Q. Feng, H. Xu, Z. Wu, and W. Liu, "Deceptive jamming detection for SAR based on cross-track interferometry," *Sensors*, vol. 18, no. 7, pp. 2265–2278, Jul. 2018.

[14] S. Zhang and L. Wen, "A new interference elimination method for multi-satellite SAR system," in *Proc. IEEE Int. Geosc. Remote Sens. Symp.*, 2008, pp. 1316–1319.

[15] W. Wang, J. Wu, J. Pei, X. Mao, and J. Yang, "An antideceptive jamming method for multistatic synthetic aperture radar based on collaborative localization and spatial suppression," *IEEE J. Sel. Topics Appl. Earth Observ. Remote Sens.*, vol. 13, pp. 2757–2768, 2020.

[16] W. Wang, J. Wu, J. Pei, Z. Sun, J. Yang, and Q. Yi, "Antirange-deception jamming from multijammer for multistatic SAR," *IEEE Trans. Geosci. Remote Sens.*, vol. 60, pp. 1–12, 2021.

[17] J. Cheng, B. Huang, W. Tang, Z. Xu, W. -Q. Wang, and S. Zhang, "A deceptive jamming against spaceborne SAR based on doppler-shift convolutional using FDA," in *Proc. Asia-Pac. Conf. Synthetic Aperture Radar*, 2019, pp. 1–5.

[18] L. Huang, Z. Zong, S. Zhang, and W. -Q. Wang, "Joint two-dimensional deception countering ISAR via frequency diverse array," *IEEE Signal Process. Lett.*, vol. 28, pp. 773–777, 2021.

[19] B. Huang, W. Wang, S. Zhang, H. Wang, R. Gui, and Z. Lu, "A novel approach for spaceborne SAR scattered-wave deception jamming using frequency diverse array," *IEEE Geosci. Remote Sens. Lett.*, vol. 17, no. 9, pp. 1568–1572, Sep. 2020.

[20] K. Yang, W. Ye, F. Ma, G. Li, and Q. Tong, "A large-scene deceptive jamming method for space-borne SAR based on time-delay and frequency-shift with template segmentation," *Remote Sens.*, vol. 12, no. 1, pp. 53–70, Dec. 2020.

[21] L. Huang, Z. Zong, S. Zhang, and W. -Q. Wang, "2-D moving target deception against multichannel SAR-GMTI using frequency diverse array," *IEEE Geosci. Remote Sens. Lett.*, vol. 19, pp. 1–5, 2020.

[22] Z. Zeng and H. Tian, "A two-dimensional mixed baseline method for recognizing deceptive jamming based on MIMO-SAR," in *Proc. Procedia Comput. Sci.*, 2020, pp. 700–705.

[23] J. Ai, Q. Luo, X. Yang, Z. Yin, and H. Xu, "Outliers-robust CFAR detector of gaussian clutter based on the truncated-maximum-likelihood-estimator in SAR imagery," *IEEE Trans. Intell. Transp. Syst.*, vol. 21, no. 5, pp. 2039–2049, May 2020.

[24] S. Xu, J. Liu, Y. Li, and Y. Fu, "A new deceptive jamming method for SAR based on false moving targets," in *Proc. Int. Conf. Radar.*, 2008, pp. 371–374.

[25] X. He, Z. Wang, and B. Tang, "Two-dimensional frequency modulation jamming to SAR based on ship-borne jammer," *Int. J. Electron. Lett.*, vol. 4, no. 2, pp. 141–157, Oct. 2016.

[26] T. Bollian, B. Osmanoglu, R. Rincon, S. Lee, and L. Fatoyinbo, "Adaptive antenna pattern notching of interference in synthetic aperture radar data using digital beamforming," *Remote Sens.*, vol. 11, no. 11, Jun. 2019, Art. no. 1346.

[27] H. Xu, Y. Zhou, and C. Li, "The analysis of baseline in spaceborne interferometric SAR," *Acta Electronica Sinica*, vol. 31, no. 3, pp. 437–439, Jul. 2003.

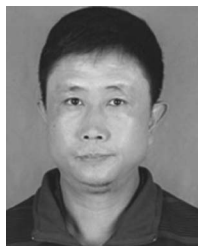

Wenhui Lang received the B.S. degree in electronic information engineering from Hefei Union University, Hefei, China, in 1987, the M.S. degree in signal and information processing from the Hefei University of Technology, Hefei, in 1993, and the Ph.D. degree in biomedical engineering from the University of Science and Technology of China, Hefei, in 2005.

He is currently an Associate Professor with the Department of Electrical Engineering, Hefei University of Technology. His research interests include signal and image processing, synthetic aperture radar countermeasures and pattern recognition.

Yaling Tang received the B.S. degree in electronic information engineering from Hefei University, Hefei, China, in 2019, and the M.S. degree in signal and information processing from Hefei University of Technology, Hefei, in 2022.

Her research interests include signal processing, synthetic aperture radar imaging and countermeasures.

Shengqun Mei received the B.S. degree in electronic information engineering from Hubei Polytechnic University, Huangshi, China, in 2019, and the M.S. degree in signal and information processing from the Hefei University of Technology, Hefei, China, in 2022.

His research interests include radar signal processing and radar countermeasure.

Fang Zhou (Member, IEEE) was born in Anhui, China. She received the B.S. and Ph.D. degrees in electrical engineering from Xidian University, Xi'an, China, in 2009 and 2014, respectively.

She is currently an Associate Professor with the School of Computer and Information, Hefei University of Technology, Hefei, China. Her research interests include synthetic aperture radar signal processing and correction.

Xuezhi Yang received the B.S. degree in electronic information engineering from Anhui University, Hefei, China, in 1992, the M.S. degree in signal and information processing from Hefei University of Technology, Hefei, in 1995, and the Ph.D. degree in pattern recognition from The University of Hong Kong, Hong Kong, in 2003.

From 2006 to 2007, he was a Postdoctoral Research Fellow with the Department of Systems Design Engineering, University of Waterloo, Waterloo, ON, Canada. He is currently a Professor and the Dean with the School of Computer and Information, Hefei University of Technology. His research interests include digital image processing, pattern recognition, and automated interpretation of synthetic aperture radar imagery.